Appendix: Parameters and theoretical model of the CNT transducer

S1. Peltier cooler efficiency and the phonon contribution to the thermal flux

The idea of the carbon nanotube Peltier cooler is shown in Fig. S1. The thermoelectric cooling

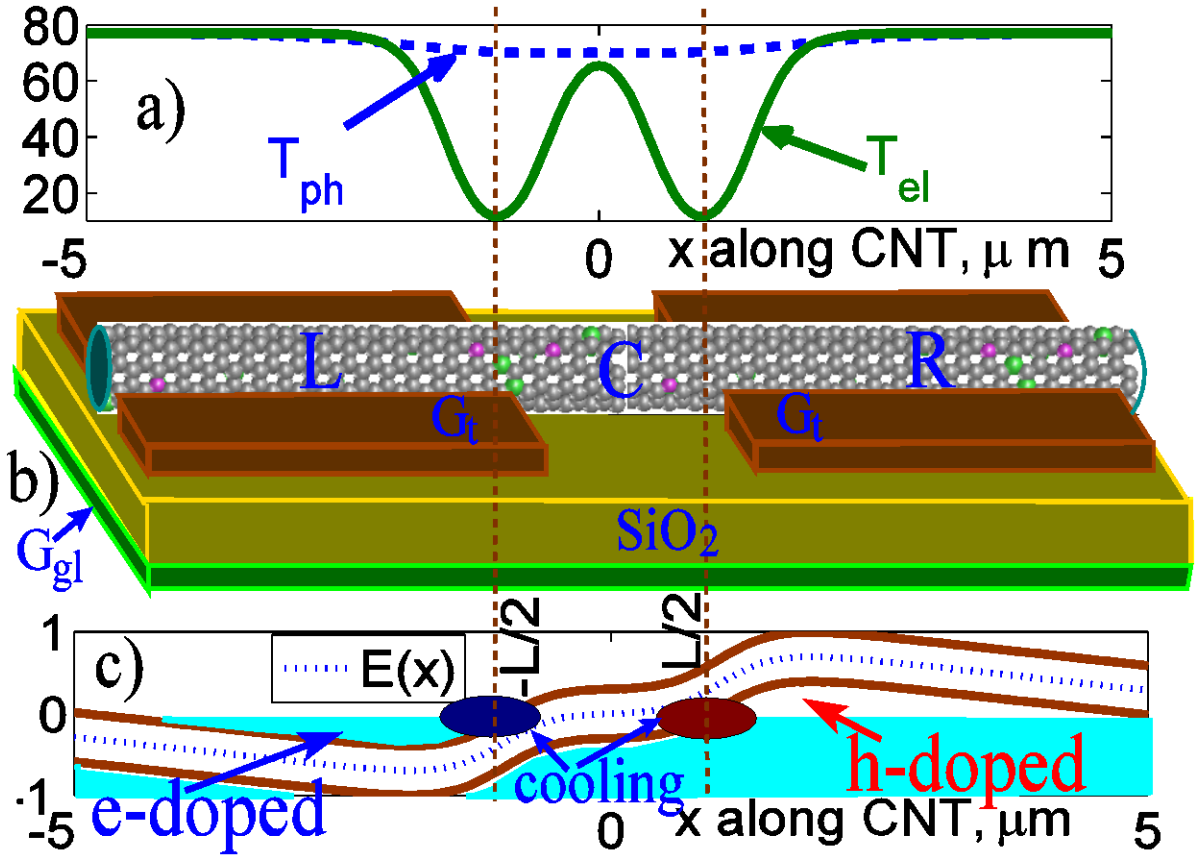

Figure S1 | Schematics of the Peltier cooling in CNT. (a) Spatial distribution of the effective temperature of electrons $T_{el}(x)$ and phonons $T_{ph}(x)$ along the CNT for the bias voltage $\Delta V = 135$ V (see calculation details in Sec. A4). The electron temperature $T_{el}(x)$ sharply drops at $-L/2 < x < L/2$ (i.e., in the active region C) owing to extraction of the electron and hole charge carriers from the C region toward the L and R sections by the flowing electric current. (b) The Peltier cooler formed by a CNT, resting on the dielectric SiO_2 substrate. G_{gl} is the global gate establishing the Fermi energy value, G_t are the local gate electrodes. (c) The voltage biased CNT structure with the electrode doping of the L and R sections. The electron spectrum becomes dependent on the coordinate x along the CNT, since its profile is set by applying the electric potentials φ_L to the G_t electrodes. The cooling takes place at the edges of the active region enclosed between the brown dash lines, in the areas denoted by the blue and red ellipses indicating where the electrons and holes respectively are created.

proceeds as follows. An electric current, flowing along the CNT from left to right, forces the electrons to the drift toward the L region, whereas the holes are drifting in the opposite direction, i.e., toward the R region. In this way, one extracts the charge carriers from the C region toward

the L and R regions, thereby creating a deficit of the hole and electron excitations in the vicinity of C. The deficiency of the electron and hole populations causes a decrease of the local effective temperature $T_{el}(x)$ of electrons at $-L/2<x<L/2$ (i.e., in the active region C) to a level far below the ambient temperature T (see the corresponding calculations in Sec. S4 below). Simultaneously, in the course of the electron-phonon collisions, considered in Sec. S2, the lowered concentration of the charge carriers tends to re-establish itself back to its equilibrium value, due to creating of new electron-hole pairs caused by absorption of the thermal phonons, thereby transferring energy from the phonon subsystem to the electron subsystem. The energy transfer process is accomplished in the course of the phonon-electron collisions as described in Sec. S4 below. Therefore, the local effective temperature $T_{ph}(x)$ of the phonon subsystem at the ends of C region also is lowered as compared to the ambient temperature T, as seen in Fig. S1a, where *x* is the coordinate along the nanotube. Thus, inside the central region C, the electrons and holes are characterized by lower effective temperature T_{el}, provided that $T>T_{ph}>T_{el}$, as shown in Fig. S1a. The precise relationship between T, T_{ph} and T_{el} depends on the amount of thermal energy, which has been transferred owing to backflow of the phonons from the L and R sections into the C section (see Fig. S2). The exact value of the transferred energy is determined by the phonon heat conductance Λ_{ph} of the charge-doped L and R sections. Because the effective temperatures T_{el} and T_{ph} of the phonon and electron subsystems differ from each other, this initializes the heat energy transfer inside the C section from the phonon subsystem to the electron subsystem.

The dimensionless figure of merit for the cooling process is defined as

$$ZT_{cold}=\frac{S^2G_e}{\Lambda}T_{cold}, \tag{S1}$$

where T_{cold} is the temperature of the cold region. The material parameters in Eq. (S1) involve Seebeck coefficient S, the electric conductance G_e and thermal conductance Λ; the parameters determine the efficiency of the Peltier cooling [1-9] in the system shown in Fig. S1. From Eq. (S1) one can see that ZT_{cold} increases with S and G_e, and decreases with Λ. On the one hand, both S and G_e are roughly proportional to the electron scattering time τ_e that depends on the CNT

purity and electron-phonon collisions [10-12]. On the other hand, in the absence of doping, the thermal conductance Λ is determined mostly by the scattering time τ_p of phonons on other phonons and also depends on the interface roughness [13-19]. In the course of propagation of the electron and hole excitations along the nanotube, they transfer part of their energy at the expense of the electron-phonon collisions to the phonon subsystem. A fraction of so excited phonons propagates along the nanotube, carrying the obtained energy away from the C section towards the nanotube ends. In the course of the reverse phonon-electron collisions [19], a fraction of the obtained energy is returned back to the electrons and holes, which eventually carry it towards the metal S and D electrodes, as denoted by the blue and pink arrows in Fig. S2.

However, there are other phonons, which do not propagate along the nanotube but escape to the substrate [20-22]. Those phonons are also responsible for the energy dissipation, since after escaping to the substrate, they disappear in the ambient environment and cannot return back to the nanotube. The relevant energy losses can be described as an effective reduction of the electron scattering time τ_e, resulting in diminishing of S and G_e, and therefore, in a reduction of the value of ZT_{cold}. We evaluate the substrate effect in Sec. S3. It is instructive to estimate the ratio of the phonons escaping into the substrate to the phonons reaching the metal electrodes. Therefore, below we discuss the phonon scattering processes determining their mean free path.

The phonon mean free path $l_{\text{p-p}}$ due to phonon-phonon collisions for three-phonon umklapp processes, assuming $\hbar\omega / k_B T >> 1$, is estimated [23] at the liquid nitrogen temperature $T = 77$ K as

$$l_{\text{p-p}} = \frac{c_m A}{\omega^2 T} \simeq 30\ \mu\text{m}, \tag{S2}$$

where $A = 3.35\times10^{23}$ m·K/s^{-2} is the coupling constant in graphene, $c_m = 0.65$ is the parameter of the CNT curvature, and a typical frequency of thermally excited phonons is $\omega = k_B T / \hbar \simeq 10^{13}$ s^{-1}. The corresponding phonon-phonon scattering rate is evaluated as

$$\Gamma_{\text{p-p}} = \hbar \frac{s}{l_{\text{p-p}}} \simeq 0.5\ \mu\text{eV}. \tag{S3}$$

The above Eq. (S2) suggests that the electron mean free path $l_{\text{p-p}}$ due to three-phonon umklapp processes is much longer than the dimensions of the L , R , and C sections, and thus such

scattering can be disregarded.

S2. Electron-restricted phonon scattering in the gated CNT sections

In the process of Peltier cooling, the phonon flux comes from the outside environment toward the active region, i.e., in the opposite direction to the propagating electrons and holes (see Fig. S2). This part of the external heat flux is diminished owing to the effect of phonon-electron collisions taking place in the charge doped CNT sections. In an undoped CNT, in the absence of charge

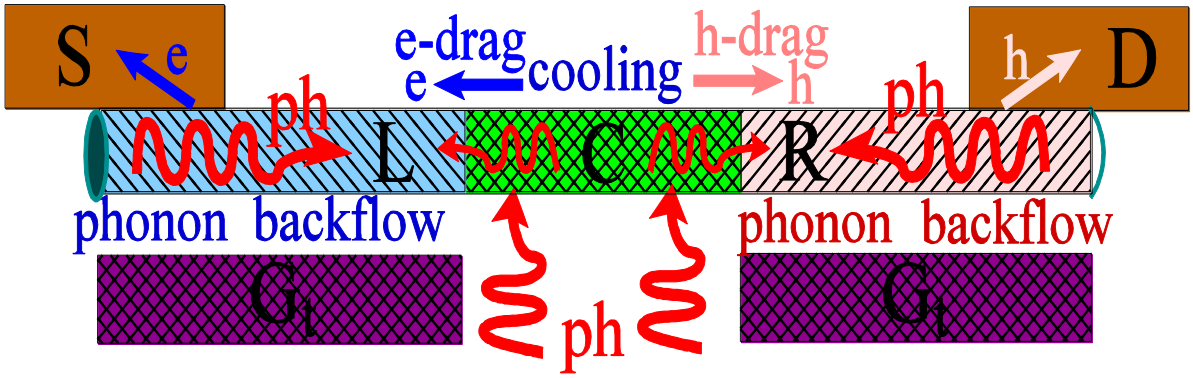

Figure S2 | Phonon transport inside the CNT Peltier cooler. The phonons are pushed out of the central cooled C region C due to collisions with the electrons drifting toward the L region of the CNT and with the holes drifting toward the R region. The corresponding microscopic mechanism is the e- and h-drag, originating from electron-phonon collisions. The electrons and holes, drifting in opposite directions under influence of the electric current, collide with phonons, thereby creating the force, which pushes the phonons toward the nanotube ends. On the contrary, since the phonon density at the nanotube ends is higher than in the central region, the backflow of phonons happens from the L and R regions toward the central C region. Owing to a high concentration of electrons in L region and holes in R region of CNT, the phonon-electron scattering causes a significant shortening of the phonon mean free path in these regions. Because the charge carrier concentration in the undoped C region is relatively low, the phonon mean free path there is large.

carriers, the phonon-electron scattering time formally is set as $\tau_{p-e} = \infty$. However, by applying the gate voltage, one introduces the charge carriers - electrons and holes - into the nanotube. Then, on the one hand, τ_{p-e} becomes finite outside the active region, since the charge carriers serve as scattering centers for the propagating phonons. On the other hand, in the undoped middle (active) region, the phonon scattering is determined by the phonon-phonon collisions, while the phonon-electron scattering is negligible. Therefore, in the middle C region, where the carriers of electric charge are absent, the phonon propagation is almost ballistic. On the contrary, outside the middle C region, where the gate voltages applied to the G_t electrodes induce the finite concentration of charge carriers in the L and R regions (see Figs. S1, S2), the phonons scatter on

the electrons and holes [19] , thereby transmitting their energy to the charge carriers. The electron concentration $n_e(x)$ versus coordinate x is assumed to have a step-wise form. To find $n_e(x)$ more accurately, one can use, e.g., the approach [24, 25]. Owing to the phonon flux from outside the cooling device, the charge carriers, coming from the middle active region, are confined to the metal S and D electrodes. For an estimation of the electron-phonon scattering rate one can use the well-known expression [26]

$$\frac{1}{\tau_{\mathrm{p-e}}} = \eta_{ps} \frac{n_e C_0^2 \omega}{\rho s^2 k_B T} \sqrt{\frac{\pi m s^2}{2 k_B T}} \exp\left(-\frac{m s^2}{2 k_B T} \right), \tag{S4}$$

where s is the acoustic phonon velocity, n_e is the concentration of conduction electrons, C_0^2 is the deformation potential, ρ is the mass density, and m is the electron effective mass, typically $m = 0.1 - 0.5 m_e$ [10-12]. The above formula (S4) is modified owing to pseudospin conservation effects [27], whose contribution is accounted for by introducing an additional factor $\eta_{\mathrm{ps}} = 0.3$. Here we assume that the phonon confinement does not strongly affect the phonon-electron scattering rates. We use that [10-12] $\rho = 7.6 \times 10^{-8}$ g/cm^2, $s = 2 \times 10^6$ cm/s, $C_0 = 19$ eV, $n_e = 3.671 \times 10^9$ m^{-1}, which gives $\tau_{\mathrm{p\text{-}e}}^{-1} = 1.5 \times 10^{11}$ s^{-1}. The effect of the global gate (which is formed at the bottom of the dielectric substrate) on n_e can be evaluated using the formula for an electric potential difference V_G between the conducting wire with diameter d and the horizontal plane separated by a distance h

$$V_G = \frac{\lambda}{2\pi\varepsilon\varepsilon_0} \ln \frac{4h}{d} \tag{S5}$$

where λ is electric charge per unit length. The above formula (S5) gives

$$\lambda = \frac{2\pi\varepsilon\varepsilon_0}{\ln(4h/d)} V_G \tag{S6}$$

Then we find the electron density per unit length n_e induced by the gate voltage V_G in the CNT as

$$n_e = \frac{2\pi\varepsilon\varepsilon_0}{e \ln(4h/D)} V_G = 3.7 \times 10^9 \frac{1}{\mathrm{m}}. \tag{S7}$$

We used that the dielectric constant of the SiO_2 substrate is $\varepsilon = 3.9$ and the gate voltage $V_G = 10\,\mathrm{V}$. Finally, for the electron density $n_e = 3.7\times10^{9}\,\mathrm{m}^{-1}$, using the CNT section length $l_e = 1-10\ \mu\mathrm{m}$, we obtain $\tau_{\mathrm{p-e}}^{-1} = 1.5\times10^{11}\ \mathrm{s}^{-1}$ and $\Gamma_{\mathrm{p-e}} = 40\ \mu\mathrm{eV}$. More generally, using the phonon-electron scattering rate $\Gamma_{p-e} = \hbar/\tau_{\mathrm{p-e}} = 0.05-0.5$ meV, we estimate the phonon mean free path $l_{\mathrm{p-e}}$ due to the phonon-electron collisions as $l_{p-e} = s\cdot\tau_{p-e} = 30-300$ nm, where we used that $s = 2.1\times10^{4}$ m/s for LA phonons. In a similar way, one describes effect of the side gates. In principle, by applying higher gate voltages, which are close to the breakdown voltage of the dielectric substrate (for the SiO_2 substrate by thickness d_{SiO2} = 300 nm the maximum gate voltage achieves ~1 kV), one can achieve much higher electron concentrations in the gated region of CNT, $n_e = 2\times10^{13}\,\mathrm{m}^{-1}$, which gives a very short phonon mean free path $l_{\mathrm{p-e}} \simeq 5-50$ nm owing to the phonon-electron collisions.

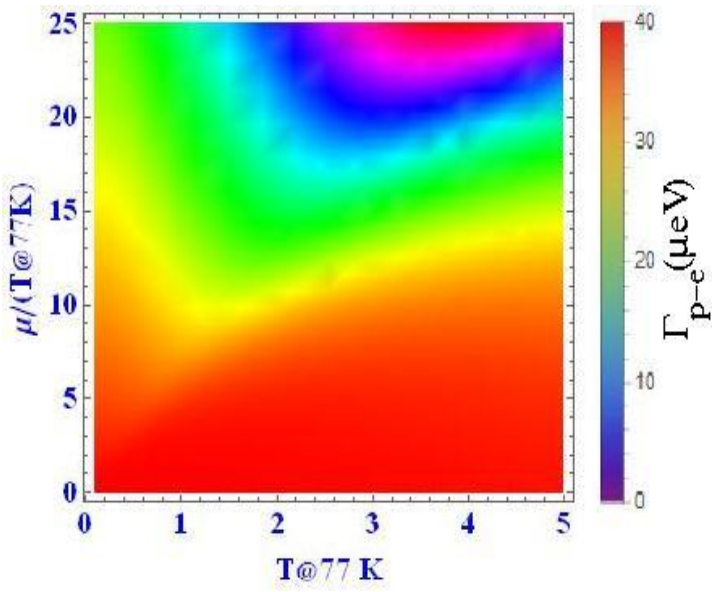

Figure S3 | The phonon-electron scattering rate $\Gamma_{\mathrm{p-e}}$ (μeV) versus effective electron temperature T_{el} in units of the liquid nitrogen temperate nitrogen temperature 77 K. One can see that the ratio $\Gamma_{\mathrm{p-e}}/\Gamma_{\mathrm{p-p}} \approx 10^{2}$, thereby suggesting that owing to the phonon-electron scattering, the phonon mean free path is shortened by two orders of magnitude, as compared to the phonon-phonon scattering mechanisms.

This allows for estimating the phonon part of the thermal conductivity restricted by the electron scattering as

$$\kappa_{\mathrm{ph}} = \frac{\rho_{2D}}{d_G}\,c\,\frac{s\cdot l_{\mathrm{ph}}}{3} = 5-50\,\frac{\mathrm{W}}{\mathrm{m}\cdot\mathrm{K}}$$

where we used the mass density of graphene $\rho_{2D} = 7.6\times10^{-8}\,\mathrm{g/cm}^2$, the graphene layer thickness $d_G = 0.34$ nm, the electron-restricted phonon mean free path $l_{p-e} = 30-300$ nm, and the specific

heat of graphene $c_G = 10\text{mJ/g}\cdot\text{K}$. The above estimate suggests that inside the L and R sections (i. e. outside the C region), where the local gate voltages are applied, the phonons transfer their energy to the electrons and holes owing to a much slower phonon group velocity ($s/v_F = 10^{-2}$). Furthermore, in the doped L and R regions, the phonon transport is effectively blocked owing to intensive phonon-electron collisions. In accordance with the Fourier law, the heat flux between the CNT and the substrate vanishes because the effective temperature of phonons T_{ph} is equal to the temperature of the substrate. Due to the aforementioned reasons, the energy transfer from the carbon nanotube to the metal electrodes outside the active region occurs solely at the expense of the electron transport.

According to Eq. (S1), other important characteristics determining the dimensionless figure of merit ZT_{cold} are the electric conductance G_e and Seebeck coefficient S. For the carbon nanotube structure sketched in Fig. S1, both G_e and S are determined by the number of conducting channels N_{ch} inside the CNT and by the transparency $\bar{T}$ of the contact between the CNT and metal electrodes, whereas the other mechanisms like the electron-phonon scattering and escape to the substrate can be neglected. This gives the conductivity

$$\sigma = \frac{L}{A}\frac{2e^2}{h}N_{\text{ch}}\bar{T} = 2\times 10^8 \frac{\text{S}}{\text{m}} \qquad \text{(S8)}$$

where we used for the gated CNT section $L = 5\ \mu\text{m}$, $\bar{T} = 0.4$, and the CNT cross section area $A = \pi d_{\text{CNT}}^2/4 = 3\text{nm}^2$ (where the CNT diameter is $d_{\text{CNT}} = 2\,\text{nm}$). According to Ref. [28], Seebeck coefficient for an undoped semiconducting CNT achieves $S \simeq 0.2\times 10^{-3}\ \text{V/K}$, which in our setup shown in Fig. S1 is improved further by using the electrode doping, yielding S up to 0.5×10^{-3} V/K. Using the above parameters, one estimates the figure of merit as high as $ZT_{cold} = 10 - 100.$

S3. Thermal flux between the CNT and the SiO_2 substrate

Part of the thermal flux, carried by the phonons, goes from the CNT into the SiO_2 substrate [20-22], while the other part is directed along the CNT. For the latter fraction, the Fourier law gives

$$q_{||} = -\kappa_{||}\frac{dT}{dx} = -\kappa_{||}\frac{T_h - T_c}{L/2} = -4.9\times 10^{11}\frac{\text{W}}{\text{m}^2}, \qquad \text{(S9)}$$

where $q_{\|}$ is the heat flux density, $\kappa_{\|} = 3600\,\mathrm{W/(m\cdot K)}$ is the heat conductivity of CNT, ∇T is the temperature gradient, and we used $T_h - T_c = 70\ \mathrm{K}$ and $L = 1\ \mu\mathrm{m}$. The corresponding heat flux along the nanotube with diameter $d_{\mathrm{CNT}} = 3\mathrm{nm}$ is $Q_x = \pi d_{\mathrm{CNT}}^2 \cdot q_x = 1.4\times10^{-5}\ \mathrm{W}$. The boundary thermal conductance, according to Ref. [29] is $\mathrm{K} = 11$ nW/K, which for the temperature difference $T_h - T_c = 70$ K gives the heat flux $Q_y = -\mathrm{K}\left(T_h - T_c\right) = 1\ \mu\mathrm{W}$. Thus, the fraction of energy, which the acoustic phonons carry from the CNT down to the substrate is

$$\frac{Q_{\perp}}{Q_{\|}} \simeq 0.1. \tag{S10}$$

Furthermore, using the known value of thermal conductance $\kappa_{\perp} = 0.014$ W/mK [30], we compute the transmission probability $\bar{\zeta}$ of the phonons through the CNT/SiO_2 interface. The phonon part of the thermal conductivity is

$$\begin{aligned} \kappa_{\perp} &= \frac{1}{2\pi\left(T_{hot} - T_{cld}\right) w_c} \int_0^{\infty} d\omega \cdot \hbar\omega \zeta_{\omega} \left(N_{\omega}^{hot} - N_{\omega}^{cld}\right) \\ &\simeq \frac{\bar{\zeta}_{\omega}}{2\pi\left(T_{hot} - T_{cld}\right) w_c} \int_0^{\infty} d\omega \cdot \hbar\omega \left(N_{\omega}^{hot} - N_{\omega}^{cld}\right), \end{aligned} \tag{S11}$$

where the non-equilibrium distribution of phonons is approximated by the Bose-Einstein function with the effective temperatures T_{h} and T_{c} for the phonon subsystems in the "cold" (c) nanotube and the "hot" (h) substrate

$$N_{\omega}^{\mathrm{h}(c)} = \frac{1}{\exp\left(\frac{\hbar\omega}{k_B T_{\mathrm{h}(c)}}\right) - 1}. \tag{S12}$$

The above Eq. (S11) allows us to estimate the average transmission probability $\bar{\zeta}$ through the CNT/SiO_2 interface as

$$\begin{aligned} \bar{\zeta}_{\omega} &= w_c \kappa_{\perp} \frac{2\pi\left(T_h - T_c\right)}{\int_0^{\infty} d\omega \cdot \hbar\omega \left(N_{\omega}^{h} - N_{\omega}^{c}\right)} \\ &= w_c \kappa_{\perp} \frac{\hbar}{\pi k_B^2} \frac{12}{T_h + T_c}, \end{aligned} \tag{S13}$$

where w_c is the effective contact width, and

$$\frac{1}{\hbar}\int_0^\infty d(\hbar\omega)\cdot\hbar\omega\left(N_\omega^{hot}-N_\omega^{cld}\right)=\frac{\pi^2k_B^2}{6\hbar}\left(T_h-T_c\right)\left(T_h+T_c\right). \tag{S14}$$

Then using, e.g., $T_h+T_c=85\,\mathrm{K}$, $\kappa_\perp=0.014\,\mathrm{W}/\left(\mathrm{m}\cdot\mathrm{K}\right)$, and the CNT/$SiO_2$ contact width $w_c=0.3\,\mathrm{nm}$, we obtain

$$\bar{\zeta}_\omega=w_c\kappa_\perp\frac{\hbar}{\pi k_B^2}\frac{12}{T_h+T_c}\simeq 0.1, \tag{S15}$$

which agrees with the estimate (S10). The above Eqs. (S10) and (S15) suggest that only a small fraction of phonons (about 10%), propagating in the electrically active region, penetrate from the CNT into the SiO_2 substrate, while most of them propagate along the CNT. However, outside the active C region, the scenario of phonon transport becomes quite different. One the one hand, abundance of the electric charge carriers in the L and R sections, serving as scattering centers for propagating phonons, causes the phonon transport along the CNT to be blocked. On the other hand, the phonon escape from the CNT into the substrate also stops, since the temperature gradient vanishes.

Besides, one can estimate the heat flux between the CNT and the SiO_2 substrate using the Fourier law and the experimental results of Refs. [20-22]. Part of the thermal flux leaks from the CNT into the SiO_2 substrate and is estimated to be

$$\vec{q}=-\kappa\nabla T \tag{S16}$$

where (in the SI units) $\vec{q}$ is the local heat flux density, Wm^{-2}, κ is the material thermal conductivity, $\mathrm{Wm}^{-1}\mathrm{K}^{-1}$, ∇T is the temperature gradient, Km^{-1}. According to Refs. [20, 21], the thermal conductance G of a stack involving the Au/Ti/graphene/SiO_2 interfaces, is defined as

$$G=\frac{\delta\vec{q}}{\delta T}=-\kappa\frac{1}{\delta x}. \tag{S17}$$

For graphene multilayers with the number of graphene layers $1\le n\le 10$ and in the temperature range of $50\le \mathrm{T}\le 500$ K they find $G\approx 25$ MW $\mathrm{m}^{-2}\mathrm{K}^{-1}$ irrespective of n at room temperature, and that the heat flow across the metal/graphene/SiO_2 interface is limited by G of the metal/graphene interface rather than by G of the graphene/SiO_2 interface. Thus, the choice of metal contacts affects both electrical and thermal transport in graphene devices. Then the thermal conductance of the graphene/SiO_2 interface is

$$\kappa_{\mathrm{G/SiO_2}} = -G\delta x = 0.025\frac{\mathrm{W}}{\mathrm{m}\cdot\mathrm{K}}, \tag{S18}$$

where we assumed the graphene/SiO_2 interface thickness $d_{G/\mathrm{SiO_2}} = 1\mathrm{nm}$. Consequently, the thermal conductance G of the Au/Ti/graphene/SiO_2 interface is

$$\kappa_{\mathrm{Ti/G/SiO_2}} = -G\delta x = 0.006\frac{\mathrm{W}}{\mathrm{m}\cdot\mathrm{K}}. \tag{S19}$$

Using the Fourier law (S9), we compare the thermal flux along the CNT relatively to the thermal flux between the CNT and substrate. One estimates the thermal flux density between the CNT and the SiO_2 substrate as

$$Q_{\perp} = -\kappa_{\perp}\frac{T_h - T_c}{d_{G/\mathrm{SiO_2}}} = 6.3\times10^{-8}\,\mathrm{W}, \tag{S20}$$

which gives the ratio

$$\frac{Q_{\perp}}{Q_{\parallel}} = \frac{6.3\times10^{-8}\,\mathrm{W}}{3.5\times10^{-6}\,\mathrm{W}} \simeq 0.02, \tag{S21}$$

where for $Q_{\parallel}$ we used the estimation (S9). This means that only ~2% or less of the total heat flux is directed between the CNT and the SiO_2 substrate. This ratio is much larger for graphene stripes, whose contact area with the SiO_2 substrate is considerably larger. Therefore, for graphene stripes, which are overlaid on the SiO_2 substrate, the ratio $Q_{\perp}/Q_{\parallel}$ achieves a few percent.

S4. Phonon drag

While the electric current passes the active region, it is carried by electrons on the left, and by holes on the right, propagating in opposite directions (see Fig. S2). If the current direction is positive, the electrons and holes are pushed away from the active region toward the metal electrodes; thus they suck the thermal energy from the active region, thereby transferring it further via the metal electrodes into the area outside of the contact. By feeding the electric current, e.g., $I = 0.01$ mA, one creates

$$\left(\frac{dn_e}{dt}\right)_{e-p} = \frac{1}{e} I = 6.2\times 10^{13}\,\frac{1}{\mathrm{s}} \tag{S22}$$

of electron-hole pairs per second. In Eq. (S22), the number of electrons created in C is $n_e = \sum_{\mathbf{p}} f_{\mathbf{p}}$, where $f_{\mathbf{p}}$ is the electron distribution function, determined by the Boltzmann equation. During their propagation, the electrons and holes transmit part of their energy to the phonons generated in the course of the electron-phonon collisions. The excited phonons propagate toward the outside area, and are eventually re-adsorbed back by the electrons and holes. However, according to Eqs. (S10), (S15), a smaller part (~10% of the total number) of propagating phonons escape from the CNT into the substrate, causing the heat flux leakage.

We assume that the leading mechanism responsible for creation of the electron and hole excitations in the active region C is determined by the electron-phonon collisions. The process of extraction of the charge carriers causes an energy drain leading to a decrease of the electron subsystem temperature T_{el}. Such extraction of the electron and hole excitations from the active region toward the metal electrodes is described by the particle balance equation

$$\sum_{\mathbf{p}} \left[\left(\frac{\partial f_{\mathbf{p}}}{\partial t} \right)_{\mathrm{extr}} - L_{\mathrm{e\text{-}p}}\left(\mathbf{p}, f_{\mathbf{p}}\right) \right] = 0 \ , \tag{S23}$$

where the first term in square brackets describes extraction of the quasiparticle electron and hole excitations from the active C region by electric current, while the second term, $L_{\mathrm{e\text{-}p}}$, is the electron-phonon collision integral in the deformation potential approximation [11, 31-35]

$$\begin{aligned} L_{\mathrm{e\text{-}p}}(\mathbf{k}, f_{\mathbf{k}}) &= \sum_{\mathbf{q}} \frac{2\left|C_q\right|^2}{\Omega\hbar^2\left|\varepsilon\left(\omega_q, \mathbf{q}\right)\right|^2} \\ &\times\{\left[f_{\mathbf{k}}\left(1- f_{\mathbf{k+q}}\right) N_{\mathbf{q}} - f_{\mathbf{k+q}}\left(1- f_{\mathbf{k}}\right)\left(1+ N_{\mathbf{q}}\right)\right]\delta\left(\varepsilon_{k+q} - \varepsilon_k - \omega_q\right) \\ &+\left[f_{\mathbf{k}}\left(1- f_{\mathbf{k-q}}\right)\left(1+ N_{\mathbf{q}}\right) - f_{\mathbf{k-q}}\left(1- f_{\mathbf{k}}\right) N_{\mathbf{q}}\right]\delta\left(\varepsilon_k - \varepsilon_{k-q} - \omega_q\right)\}. \end{aligned} \tag{S24}$$

The above Eqs. (S23), (S24) are complemented by the energy balance equations taking into account that the *e*- and *h*-excitations are created in the course of the electron-phonon collisions. The phonon energy loss rate per unit volume is found using the relation [36]

$$P = \frac{1}{\Omega}\sum_q \hbar\omega_q \frac{dN_q}{dt} + P_{esc}, \tag{S25}$$

where Ω is the normalizing volume, and P_{esc} is the heat leakage owing to the phonon escape into the substrate. Assuming that the leading contribution to dN_q/dt in Eq. (S25) comes from the phonon-electron collisions [32, 37], one writes

$$\begin{aligned}\frac{dN_q}{dt} \simeq & \frac{2\left|C_q\right|^2}{\Omega\hbar^2\left|\varepsilon\left(\omega_q,\mathbf{q}\right)\right|^2} \\ & \times\sum_{\mathbf{k}}\{\left[f_{\mathbf{k}}\left(1-f_{\mathbf{k+q}}\right)N_{\mathbf{q}}-f_{\mathbf{k+q}}\left(1-f_{\mathbf{k}}\right)\left(1+N_{\mathbf{q}}\right)\right]\delta\left(\varepsilon_{k+q}-\varepsilon_k-\omega_q\right) \\ & +\left[f_{\mathbf{k}}\left(1-f_{\mathbf{k-q}}\right)\left(1+N_{\mathbf{q}}\right)-f_{\mathbf{k-q}}\left(1-f_{\mathbf{k}}\right)N_{\mathbf{q}}\right]\delta\left(\varepsilon_k-\varepsilon_{k-q}-\omega_q\right)\}.\end{aligned} \tag{S26}$$

Furthermore, for calculating P, we assume that the electron-electron collisions are sufficiently frequent in order to provide the use of the electron temperature approximation for the electrons. Using the above expressions (S25), (S26), one finds

$$\begin{aligned}P = & \sum_q \frac{2\left|C_q\right|^2}{\left(\Omega\hbar\right)^2\left|\varepsilon\left(\omega_q,\mathbf{q}\right)\right|^2}\hbar\omega_q\left[N_q-N_q^{(c)}\right] \\ & \times\sum_k\left[f_k^{(c)}-f_{k+q}^{(c)}\right]\delta\left(\varepsilon_{k+q}-\varepsilon_k-\omega_q\right),\end{aligned} \tag{S27}$$

where N_q is the distribution function of "hot" phonons, $N_q^{(c)}$ is the distribution function of "cold" phonons, and $f_k^{(c)}$ is the distribution function of "cold" electrons. Next, we replace the summation in Eq. (S27) by integration as

$$\begin{aligned}& \sum_k\left[f_k^{(c)}-f_{k+q}^{(c)}\right]\delta\left(\varepsilon_{k+q}-\varepsilon_k-\omega_q\right) \\ & \to\int d\varepsilon_k g\left(\varepsilon_k\right)\left[f_{\varepsilon_k}^{(c)}-f_{\varepsilon_k+\omega_q}^{(c)}\right]\delta\left(v_F q+\frac{\hbar}{2m}q^2-\omega_q\right),\end{aligned} \tag{S28}$$

where the finite electron mass m arises due to presence of electron subbands (in the CNT, typically $m=0.1-0.5m_e$) and $g\left(\varepsilon\right)$ is the 1D electron density of states in the carbon nanotube [38]

$$g\left(\varepsilon\right)=\frac{\sqrt{3}}{\pi^2}\frac{1}{\left|V_{pp\pi}\right|}\frac{d}{r}\sum_{m=1}^{N}\mathbf{Re}\left(\frac{\left|\varepsilon\right|}{\sqrt{\varepsilon^2-\varepsilon_{\mathbf{m}}^2}}\right), \tag{S29}$$

where d is the carbon-carbon bond distance ($a=d\sqrt{3}$) and r is the nanotube radius ($\left|R\right|=2\pi r$). We use

$$\varepsilon_{k+q}-\varepsilon_k=\frac{\hbar^2\left(k_F+q\right)^2}{2m}-\frac{\hbar^2k_F^2}{2m}$$
$$=\frac{\hbar^2k_Fq}{m}+\frac{q^2\hbar^2}{2m}\simeq v_F\hbar q+\frac{\hbar^2}{2m}q^2, \tag{S30}$$

where $v_F=\hbar k_F/m$, which gives

$$\int\left[f_\varepsilon^{(c)}-f_{\varepsilon+\omega}^{(c)}\right]d\varepsilon\simeq T\log\left(\frac{2e^{\frac{\omega_q}{T_c}}}{e^{\frac{\omega_q}{T_c}}+1}\right). \tag{S31}$$

Using the above formulas (S28)-(S30), Eq. (S27) is rewritten as

$$P=N(0)T_c\frac{2\left|C_0\right|^2}{\left(\Omega\hbar\right)^2\left|\varepsilon_{ph}^0\right|^2}\sum_q\hbar\omega_q\left[\frac{1}{e^{\frac{\omega_q}{T_h}}-1}-\frac{1}{e^{\frac{\omega_q}{T_c}}-1}\right]$$
$$\times\log\left(\frac{2e^{\frac{\omega_q}{T_c}}}{e^{\frac{\omega_q}{T_c}}+1}\right)\delta\left(v_Fq+\frac{\hbar}{2m}q^2-\omega_q\right). \tag{S32}$$

The last Eq. (S32) allows one to compute the loss rate of thermal energy transmitted from "hotter" phonons with the temperature T_h to the colder electrons characterized by an effective temperature T_c due to their expulsion from the active region caused by the flowing electric current. The integral (S32) is simplified to the form

$$P=N(0)T_c\frac{2\left|C_0\right|^2}{\left(\Omega\hbar\right)^2\left|\varepsilon_{ph}^0\right|^2}\int_0^{\omega_D}d\omega_qF\left(\omega_q\right)\hbar\omega_q\left[\frac{1}{e^{\frac{\omega_q}{T_h}}-1}-\frac{1}{e^{\frac{\omega_q}{T_c}}-1}\right]$$
$$\times\log\left(\frac{2e^{\frac{\omega_q}{T_c}}}{e^{\frac{\omega_q}{T_c}}+1}\right)\delta\left(v_Fq+\frac{\hbar}{2m}q^2-\omega_q\right) \tag{S33}$$
$$\simeq N(0)T_c^2\frac{2\left|C_0\right|^2}{\left(\Omega\hbar\right)^2\left|\varepsilon_{ph}^0\right|^2}F\left(\omega_q^{(1)}\right)\Phi(T_h,T_c)$$

where $\hbar\omega_q^{(1)}=2p_Fs$, s is the sound velocity and $F\left(\omega_q\right)$ is the phonon density of states, and factor

$$\Phi(\lambda)=x\left[\frac{1}{e^{x/\lambda}-1}-\frac{1}{e^x-1}\right]\log\left(\frac{2e^x}{e^x+1}\right), \tag{S34}$$

and

$$x=\frac{2mv_F s}{k_B T_c},\ \lambda=\frac{T_h}{T_c},\ \frac{2mv_F s}{k_B T_c}\frac{T_c}{T_h}=\frac{x}{\lambda}, \tag{S35}$$

where $v_F=2\times10^6\,\mathrm{m/s}$ is the Fermi velocity and $s=2\times10^6\,\mathrm{cm/s}$ is the sound velocity in the CNT. In the above equations, the screening effects were introduced by dividing the matrix elements C_0 by the dielectric function of graphene ε_{ph}^0. Taking into account that the matrix elements in graphene are determined by the change in the overlap between the orbitals surrounding different atoms and not by a Coulomb potential, we set $\varepsilon_{ph}^0=1$. Depending on the geometry and on the ratio $T_h/T_{cld}=1-100$, $\Phi(\lambda,x)$ achieves values of $10-10^3$, which gives an estimate $P\simeq0.1-10$ nW.

The above estimation was obtained assuming that the "hot" temperature $T_h=77\,\mathrm{K}$ and the "cold" temperature $T_c=0.8-8\,\mathrm{K}$. Furthermore, we assumed that phonon confinement does not influence the phonon-electron scattering rates. Here we used the same parameters [10, 35, 39] as listed above in Eq. (S4) and

$$g(0)\simeq\frac{\sqrt{3}}{\pi^2}\frac{1}{\left|V_{pp\pi}\right|}\frac{2d_{\mathrm{cc}}}{d_{CNT}}=6.6454\times10^{-3}\frac{1}{\mathrm{eV}} \tag{S36}$$

where $d_{\mathrm{cc}}=0.142$ nm is the spacing of the carbon atom bonds ($a=d_{\mathrm{cc}}\sqrt{3}$), $V_{pp\pi}\approx2.5\,\mathrm{eV}$ is the nearest-neighbor pp interaction.

Inside the active C-region, the “hot” temperature T_{ph} of the phonon subsystem, as well as the “cold” temperature T_{el} of the electron subsystem, are computed using the above particle and energy balance equations (S23) and (S25). Typical result of the numeric calculations is shown in Fig. S1a. In this scenario, the energy deficit of the electron subsystem is compensated by the energy obtained from the phonon subsystem in the course of the electron-phonon collisions. Furthermore, the electron-phonon scattering cause generation of a sufficient number of the new electron-hole pairs to maintain the electric current, which is accompanied by the outflow of charge carries from the active region. Using the energy and quasiparticle balance equations, we obtain two conditions determining the local effective temperature of electrons T_{el} and phonons T_{ph} inside the active region.

Taking into account that the mean free path $l_{e(h)}$ of the electrons (*e*) and holes (*h*) in the active region is about $l_{e(h)} = 1.3\ \mu\text{m}$, we conclude that the change carriers, while propagating in the active region, transfer a smaller part (<7%) of their energy to phonons. The larger fraction (>93%) of the electrons and holes reaches the area outside the active region and goes to the metal electrodes. The phonon mean free path l_{p-p} in the active region is determined mostly by the phonon-phonon scattering, which is relatively weak, therefore l_{p-p} exceeds the length of the active region, i.e., $l_{p-p} > 1\mu\text{m}$, meaning that phonons practically do not collide with electrons and holes inside the neutral active region in the C section. Instead, a larger fraction (>90%) of phonons propagates along the nanotube, while their smaller part (<10%) goes into the SiO_2 substrate. Upon reaching the gated sections of the nanotube, the phonons collide there with the charge carriers, and their mean free path becomes very short ($l_{p-e} < 0.3\mu\text{m}$). For such reasons, the phonons quickly transfer their energy to the charge carriers which tunnel from the CNT into the metal electrodes thereafter.

S5. Quantum capacitance

In the experiments with the carbon nanotube field effect transistors (FET), the effect of the capacitance [40-42] is evaluated as follows. Knowing the length of a device, one obtains a gate efficiency (typically α_1 = 0.1-1%), which allows one to determine the quantum capacitance of the nanotube C_q using the equation

$$C_q = C_{ge}\frac{1-\alpha}{\alpha}, \tag{S37}$$

where $C_{ge} \approx 2\pi\varepsilon L / \ln\left(4h/d\right)$ is the geometry capacitance of the nanotube, *h* is the thickness of the dielectric SiO_2 between the doped Si substrate and the nanotube, $\varepsilon = 3.9\varepsilon_0$ for SiO_2, and *d* is the diameter of the nanotube. Typical geometry capacitance of the CNT device is ~10 aF, and the quantum capacitance is C_q~1000-2000 aF.

The total voltage change is the sum of these two contributions. Therefore, the total effect is *as if* there are two capacitances in series: The conventional geometry-related capacitance C_{ge} (as calculated by the Gauss law), and the "quantum capacitance" C_q related to the density of

states [40-42]. The latter is

$$C_q = e^2 N(0), \tag{S38}$$

where $N(0)$ is the electron density of states at the Fermi level (S36). Eqs. (S37), (S38) suggest that neither the geometrical capacitance C_{ge} nor the quantum capacitance C_q depend on temperature, since the electron density of states $N(0)$ is temperature-independent. A thorough derivation of formula for C_q shows that the temperature dependence basically is pronounced as a change of the width $\Gamma(T)$ of sharp peaks, occurring in the dependence of electric differential conductance $G_e(V_{SD})$ versus the source-drain bias voltage V_{SD}. A most essential contribution to $\Gamma(T)$ originates from the inelastic processes of the electron-phonon scattering, which are responsible for the energy dissipation in the system. An inelastic effect of the electron-phonon scattering is accounted by replacing in Eq. (S29) the electron energy as $\varepsilon \to \varepsilon + i\Gamma(T)$, which results in the temperature dependence of the electron spectral singularities, and can be observed experimentally by measuring the electric differential conductance $G_e(V_{SD})$. Therefore, the temperature dependence of the electron peak width $\Gamma(T)$, after a proper calibration, can be used as a meter for monitoring the effective electron temperature T_{el}. This approach is used in our work to determine the effect of intrinsic cooling in our CNT FET setup.

References

1. Hicks, L. D.; Dresselhaus, M. S. *Phys Rev B* **1993,** 47, (24), 16631-16634.
2. Hicks, L. D.; Dresselhaus, M. S. *Phys Rev B* **1993,** 47, (19), 12727-12731.
3. Hicks, L. D.; Dresselhaus, M. S. *Semiconductor Heterostructures for Photonic and Electronic Applications* **1993,** 281, 821-826.
4. Lin, Y. M.; Sun, X. Z.; Dresselhaus, M. S. *Phys Rev B* **2000,** 62, (7), 4610-4623.
5. Zhang, Z. B.; Sun, X. Z.; Dresselhaus, M. S.; Ying, J. Y.; Heremans, J. *Phys Rev B* **2000,** 61, (7), 4850-4861.
6. Shafranjuk, S. E. *Epl-Europhys Lett* **2009,** 87, (5).
7. Shafranjuk, S. E. *European Physical Journal B* **2014,** 87, (4).

8. Mayle, S.; Gupta, T.; Davis, S.; Chandrasekhar, V.; Shafraniuk, S. *J Appl Phys* **2015,** 117, (19).
9. Shafraniuk, S., *Graphene: Fundamentals, Devices and Applications*. Pan Stanford: 2015; p 634.
10. Adam, S.; Hwang, E. H.; Das Sarma, S. *Physica E-Low-Dimensional Systems & Nanostructures* **2008,** 40, (5), 1022-1025.
11. Hwang, E. H.; Das Sarma, S. *Phys Rev B* **2008,** 77, (11).
12. Hwang, E. H.; Das Sarma, S. *Phys Rev B* **2008,** 77, (8).
13. Gautreau, P.; Chu, Y. B.; Ragab, T.; Basaran, C. *Computational Materials Science* **2015,** 103, 151-156.
14. Chu, Y. B.; Gautreau, P.; Basaran, C. *Appl Phys Lett* **2014,** 105, (11).
15. Gautreau, P.; Ragab, T.; Chu, Y. B.; Basaran, C. *J Appl Phys* **2014,** 115, (24).
16. Gautreau, P.; Ragab, T.; Basaran, C. *Carbon* **2013,** 57, 59-64.
17. Gautreau, P.; Ragab, T.; Basaran, C. *J Appl Phys* **2012,** 112, (10).
18. Lindsay, L.; Broido, D. A. *Phys Rev B* **2010,** 82, (20).
19. Zou, J.; Balandin, A. *J Appl Phys* **2001,** 89, (5), 2932-2938.
20. Koh, Y. K.; Bae, M. H.; Cahill, D. G.; Pop, E. *Nano Letters* **2010,** 10, (11), 4363-4368.
21. Cahill, D. G.; Braun, P. V.; Chen, G.; Clarke, D. R.; Fan, S. H.; Goodson, K. E.; Keblinski, P.; King, W. P.; Mahan, G. D.; Majumdar, A.; Maris, H. J.; Phillpot, S. R.; Pop, E.; Shi, L. *Applied Physics Reviews* **2014,** 1, (1).
22. Hsieh, W. P.; Lyons, A. S.; Pop, E.; Keblinski, P.; Cahill, D. G. *Phys Rev B* **2011,** 84, (18).
23. Yamamoto, T.; Konabe, S.; Shiomi, J.; Maruyama, S. *Applied Physics Express* **2009,** 2, (9).
24. Ramu, A. T.; Cassels, L. E.; Hackman, N. H.; Lu, H.; Zide, J. M. O.; Bowers, J. E. *J Appl Phys* **2011,** 109, (3).
25. Ramu, A. T.; Cassels, L. E.; Hackman, N. H.; Lu, H.; Zide, J. M. O.; Bowers, J. E. *J Appl Phys* **2010,** 107, (8).
26. Parrott, J. E. *Revue Internationale Des Hautes Temperatures Et Des Refractaires* **1979,** 16, (4), 393-403.
27. Ando, T. *Journal of the Physical Society of Japan* **2005,** 74, (3), 777-817.
28. Nakai, Y.; Honda, K.; Yanagi, K.; Kataura, H.; Kato, T.; Yamamoto, T.; Maniwa, Y. *Applied Physics Express* **2014,** 7, (2).

29. Marconnet, A. M.; Panzer, M. A.; Goodson, K. E. *Reviews of Modern Physics* **2013,** 85, (3), 1295-1326.
30. Chen, L.; Kumar, S. *Journal of Heat Transfer-Transactions of the Asme* **2014,** 136, (5).
31. Ziman, J. M. *Philosophical Magazine* **1965,** 11, (110), 438-&.
32. Ziman, J. M., *The Theory of Transport Phenomena in Solids*. Clarendon Press: Oxford, 1960.
33. Hwang, E. H.; Adam, S.; Das Sarma, S. *Phys Rev Lett* **2007,** 98, (18).
34.Hwang, E. H.; Das Sarma, S. *Phys Rev B* **2007,** 75, (20).
35. Hwang, E. H.; Das Sarma, S. *Phys Rev B* **2008,** 77, (19).
36. Bockelmann, U.; Bastard, G. *Phys Rev B* **1990,** 42, (14), 8947-8951.
37. Ziman, J. M. *Philosophical Magazine* **1956,** 1, (2), 191-198.
38. Mintmire, J. W.; White, C. T. *Phys Rev Lett* **1998,** 81, (12), 2506-2509.
39. Hwang, E. H.; Das Sarma, S. *Phys Rev Lett* **2008,** 101, (15).
40. Ilani, S.; Donev, L. A. K.; Kindermann, M.; McEuen, P. L. *Nature Physics* **2006,** 2, (10), 687-691.
41. Parkash, V.; Goel, A. K. *Nanoscale Research Letters* **2010,** 5, (9), 1424-1430.
42. Parkash, V.; Goel, A. K. *2010 International Conference on Microelectronics* **2010**, 244-247.